GEOFISICA

INTERNACIONAL

REVISTA DE LA UNION GEOFISICA MEXICANA, AUSPICIADA POR EL INSTITUTO DE GEOFISICA DE LA UNIVERSIDAD NACIONAL AUTONOMA DE MEXICO

Vol. 15

México, D. F., 1o. de enero de 1975

Núm. 1

CASE STUDIES OF FRICTIONAL DISSIPATION IN NUMERICALLY SIMULATED CLOUDS

FRANCIS P. RICHARDS* and GEIRMUNDUR ARNASON**

RESUMEN

Se investigan, por medio de un modelo bidimensional, los efectos de la difusión turbulenta parametrizada de calor y cantidad de movimiento. Los experimentos numéricos incluyen, tanto coeficientes de intercambio constantes, como variables y los resultados se comparan con aquellos experimentos en los que la difusión no se incluye.

La comparación demuestra que sin difusión turbulenta el desarrollo simulado de las nubes es irrealmente intenso. En contraste, ambos tipos de difusión turbulenta simulada evitan desarrollos excesivos y producen nubes cuyas características generales son similares a las de las nubes observadas.

De los dos tipos de difusión parametrizada, la de coeficiente de intercambio variable parece dar los mejores resultados. Esto se refleja en un estado inicial, más realista, del desarrollo de las nubes y en una incorporación lateral turbulenta del aire, más fuerte cerca de las fronteras de las nubes, la cual está de acuerdo con las observaciones.

ABSTRACT

The effects of parameterized eddy diffusion of heat and momentum in numerically simulated convective clouds are investigated by means of a two-dimensional model. The numerical experiments include both variable and constant exchange coefficients, and the results are compared with those of experiments where diffusion is omitted altogether.

The comparison shows that without eddy diffusion the simulated cloud development is unrealistically intense. In contrast, both types of simulated eddy diffusion prevent excessive

^{*} Center for Experiment Design and Data Analysis, Environmental Data Service, NOAA, Washington, D. C.

^{**} Department of Atmospheric Science, State University of New York at Albany, Albany, New York 12222.

developments and produce clouds whose overall features are similar to those of observed clouds.

Of the two types of parameterized diffusion, the one whose eddy exchange coefficient is variable appears to give the best results. This is reflected in a more realistic initial stage of cloud development and stronger turbulent entrainment near cloud boundaries in agreement with observations.

INTRODUCTION

A number of numerical models simulating various aspects of atmospheric convection have been developed in recent years. These have for the most part been limited to either one or two space dimensions and have to a varying degree included the physics of clouds and precipitation. A vexing problem has always been the inclusion of eddy diffusion of heat and momentum. Because this process takes place on scales smaller than can be resolved directly by the models, parameterization of some kind is unavoidable. Some of the earlier work on one-dimensional models used a quite simple approach in which the diffusion term relating to a physical variable was proportional to the first or second power of that variable. This includes entrainment coefficients, based on laboratory experiments or similarity theory, inversely proportional to cloud radius. Such an approach is primarily aimed at simulating the effects of dynamic entrainment as opposed to turbulent dissipation, although a distinction between the two can not be clearly drawn in such a simple model.

By adding one more dimension, dynamic entrainment is satisfactorily handled by means of the continuity equation, whereas eddy diffusion requires some form of parameterization. This usually draws on concepts such as mixing length hypothesis and forms of viscous terms as they appear in molecular theory for viscosity, including the use of a constant eddy exchange coefficient. Parameterization of this kind appears to be tolerably realistic and in numerical simulation it has the added benefit of suppressing spurious developments exclusively related to the numerical process.

The present paper is a case study of a cloud simulated by means of a two-dimensional model in which a nonlinear exchange coefficient is being used. More specifically, the exchange coefficient is a function of both the grid separation and the shearing deformation as proposed by Smagorinsky (1963). Lilly (1962) was the first to use this approach in the convection problem. Wilhelmson and Ogura (1972) also used it in their study of the pressure perturbation associated with convection. A similar formulation, depending also on the Richardson number, was employed by Drake *et al.* (1974). Steiner (1973) and Wilhelmson (1974) incorporated this formulation in their three-dimensional models.

Here we shall compare two frictional parameterizations, one using a constant and the other a variable exchange coefficient; both are compared with a case where eddy diffusion is omitted altogether.

To provide a simple framework in which to study the effects of the frictional parameterization, a series of experiments modeling dry convection is first conducted. Subsequently, moist convection is simulated using an actual sounding from the Caribbean, and the results are compared to available cloud observations.

THE MODEL

The model is that described by Arnason et al. (1968) with the addition of parameterized eddy diffusion of heat and momentum. The equations of motion (vorticity equation), thermodynamics, continuity, and equations for bulk physics parameterization of cloud and precipitation processes are solved numerically. The model is a two-dimensional (x, z plane) slab-symmetric model extending 3 km in the vertical and 6 km in the horizontal. Because of imposed symmetry in the horizontal about a center plane, x = 0, solution for only one-half of the domain is necessary; all variables in the other half are either symmetric or anti-symmetric. A mesh length of 100 m is used in both the x and z directions, and the maximum time step is 15 sec. The initial conditions consist of a basic state whose variables are functions of z only and superimposed perturbations which are functions of x, z, and t. In all the experiments there is initially no motion. In the equations that follow, a zero subscript refers to a

basic state variable and quantities without a subscript are deviations from the basic state except q_v which denotes the total mixing ratio; a complete list of symbols appears in Appendix A. The relevant equations are:

$$\frac{\mathrm{d}\zeta}{\mathrm{d}t} - g \frac{\partial B}{\partial x} = \frac{\partial^2 \tau_{XZ}}{\partial x^2} - \frac{\partial^2 \tau_{ZX}}{\partial z^2} + \frac{\partial^2 \tau_{ZZ}}{\partial x \partial z} - \frac{\partial^2 \tau_{XX}}{\partial x \partial z}$$
(1)

$$\xi = \frac{\partial^2 \psi}{\partial x^2} + \frac{\partial^2 \psi}{\partial z^2} \tag{2}$$

$$\frac{d\theta}{dt} + \frac{\partial \psi}{\partial x} \frac{\partial \theta_0}{\partial z} = \frac{\partial}{\partial x} \left(K_H \frac{\partial \theta}{\partial x} \right) + \frac{\partial}{\partial z} \left(K_H \frac{\partial \theta}{\partial z} \right) + \frac{\theta_0}{c_p T_0} (\delta_0 Q_1 \dots$$

$$+ \delta_3 Q_2) \tag{3}$$

$$\frac{\partial^2 p}{\partial x^2} \, + \, \frac{\partial^2 p}{\partial z^2} \, + \, 2 \rho_0 [(\frac{\partial^2 \psi}{\partial x \partial z})^2 \, - \, \frac{\partial^2 \psi}{\partial x^2} \, \frac{\partial^2 \psi}{\partial z^2}] \, + \, g \rho_0 \, \, \frac{\partial B}{\partial z} \, = \,$$

$$\rho_0 \frac{\partial^2 \tau_{XX}}{\partial z^2} + 2\rho_0 \frac{\partial^2 \tau_{XZ}}{\partial x \partial z} + \rho_0 \frac{\partial^2 \tau_{ZZ}}{\partial x^2}$$
 (4)

$$\frac{\mathrm{dq_V}}{\mathrm{dt}} = \delta_0 S_0 + \delta_3 S_3 \tag{5}$$

$$\frac{\mathrm{dq}_{\mathrm{c}}}{\mathrm{dt}} = - \delta_{\mathrm{0}} S_{\mathrm{0}} - \delta_{\mathrm{1}} S_{\mathrm{1}} - \delta_{\mathrm{2}} S_{\mathrm{2}} \tag{6}$$

$$\frac{dq_p}{dt} = \delta_1 S_1 + \delta_2 S_2 - \delta_3 S_3 - S_4 \tag{7}$$

$$\frac{\partial}{\partial t} \int \rho_{0}(K_{E} + P_{E})d\sigma + \int \rho_{0}\phi \left[\frac{(L - c_{p}T_{0})(\delta_{0}Q_{1} + \delta_{3}Q_{2})}{c_{p}T_{0}L} + \dots \right]$$

$$\frac{\partial}{\partial z}(q_{p}V) d\sigma + \int \left[\frac{\rho_{0}\phi}{\theta_{0}}(K_{H}\nabla^{2}\theta + \frac{\partial K_{H}}{\partial x}\frac{\partial \theta}{\partial x} + \frac{\partial K_{H}}{\partial z}\frac{\partial \theta}{\partial z}) + \dots \right]$$

$$+ \rho_{0}\epsilon d\sigma = 0 \tag{8}$$

In the vorticity equation (1) B, the buoyancy, is a function of both the temperature perturbation and the suspended liquid water, and τ_{ij} are the stress components. In the potential temperature equation (3), K_H is the eddy exchange coefficient for heat, Q_1 represents heat gained from release of latent heat of condensation or heat lost through evaporation of cloud drops, and Q_2 is the loss of heat due to evaporation of rain. The pressure equation (4) is purely diagnostic in nature. The lack of uniqueness of solution to this equation for appropriate boundary conditions was first discussed by Ogura and Charney (1962) within a strictly dynamic framework. More recently Árnason (1974) has shown how uniqueness may be achieved when kinematic and thermodynamic constraints of the model are taken into account. It suffices here to point out that the solution used in this paper contains an arbitrary constant which was set equal to zero for the purpose of these experiments.

The next three equations (5) - (7) are for water substance in its various forms. They are expressions for conservation of water substance, with fallout of precipitation as the only possible sink. The mixing ratio q_V in (5) can change by condensation or evaporation of cloud drops (S₀) and by the evaporation of falling rain (S₃). The cloud mixing ratio q_C in (6) can change by condensation or evaporation (S₀), autoconversion of cloud drops to rain (S₁) and by coalescence with raindrops (S₂). The precipitation mixing ratio q_D in (7) may change by autoconversion (S₁), coalescence (S₂), evaporation (S₃) and by fallout (S₄). The tags δ_i (i = 0, 1, 2, 3) indicate the presence ($\delta_i = 1$) or absence ($\delta_i = 0$) of the source terms; decisions

criteria, definition of the source terms and their relations to parameterized cloud physics is dealt with in Appendix B.

It is to be noted that eddy diffusion terms are not included in the equations for water substance. While there are no compelling reasons for this omission in the equations for specific humidity and specific water content, most modelers find that in the precipitation equation (7), the rain is spread out too much when diffusion is included. Murray (1965) also felt that using an exchange coefficient as large as that for momentum also spread out the other moisture fields too much. He used a much smaller coefficient for water substance than for momentum. Because of doubt as to the proper choice of an exchange coefficient, no explicit diffusion terms were used in the moisture equations. Only the slight implicit smoothing of the Lax-Wendroff scheme and the application of an explicit smoother designed specifically to suppress short wave phenomena (Shuman, 1957) provided mixing effects in the moisture equations.

The energy equation (8) is formed by multiplying the first equation of motion by u and the second by w, adding them, and then making use of the thermodynamic equation, the continuity equation, and relations from the bulk physics parameterization. The details of the derivation are dispensed with. The first integral contains total kinetic and potential energies where K_E and P_E are kinetic and potential energies per unit mass. The next integral is composed of a source term due to latent heat of phase transformation and a term which expresses the energy contained in rain falling with a velocity V. In the course of the experiment this last term involving the falling rain was always at least three orders of magnitude smaller than the dominant term and could have been neglected. The last integral contains terms stemming from dissipation of heat (temperature terms) and momentum, the latter represented by the dissipation function ϵ .

A leap-frog finite-difference scheme with centered space differences is used to solve the vorticity equation. Once the new vorticity is predicted, the stream function ψ is found by solving Eq. (2) by the method of successive over-relaxation. From knowledge of the stream

function field, the components of the velocity may be determined from the relations

$$u = -\partial \psi / \partial z$$
 and $w = \partial \psi / \partial x$

which satisfy the continuity equation

$$\partial u/\partial x + \partial w/\partial z = 0.$$

Using these predicted velocities the temperature equation and the moisture equations are solved using a two-step Lax-Wendroff scheme. The pressure equation is independent of the above set of equations and may be solved at any time step.

The kinematic boundary conditions require that the normal components of the velocity vanish at the boundaries which in turn determines the stream function at the boundaries. The boundary conditions for the pressure equation are found from the equations of motion by setting the total time rate of change of velocity zero. Vorticity is specified as being zero at the external boundaries and because of the symmetry conditions it is zero for x = 0 where also u = 0 for the same reason. Since the symmetry boundary x = 0, is an internal boundary, frictional stress has to be determined, the details of which will be considered in the next section. In mathematical terms the appropriate boundary conditions are:

$$z = 0, H$$
 : $\psi = \zeta = w = 0$, $\frac{\partial p}{\partial z} = \rho_0 g B + \rho_0 \frac{\partial \tau_{XZ}}{\partial x} \dots$

$$+ \rho_0 \frac{\partial \tau_{ZZ}}{\partial x}$$
 (9)

$$z = H: q_p = 0$$

$$x = 0, \pm L$$
 : $\psi = \zeta = u = 0$, $\frac{\partial p}{\partial x} = \rho_0 \frac{\partial \tau_{XX}}{\partial x} + \rho_0 \frac{\partial \tau_{ZX}}{\partial z}$

In the continuity equation of this model, the local time rate of density is omitted. Ogura and Charney (1962) have shown that this successfully eliminates sound waves. They also analyzed the stability requirements for a system similar to that used in the present model. Their criteria were adopted with some modification. The condition for computational instability due to gravity waves in their analysis depends on assuming either that $\Delta x/\Delta z \ll 1$ or $\Delta x/\Delta z \gg 1$, corresponding to two limiting cases, In the present model these correspond to maximum time steps of 92.5 and 19.5 sec respectively. Both criteria were satisfied by allowing a maximum time step of 15 sec. It was necessary, however, to modify their criteria for the advective terms due to the use of the Lax-Wendroff scheme. As shown by Árnason and Newburg (1966) the appropriate condition then becomes

$$\Delta t \leq \left[\delta \left(\frac{u}{\Delta x} + \frac{w}{\Delta z}\right)\right]^{-1} \tag{10}$$

where $\delta = \sqrt{2}$ or $\delta = 1$. depending on whether the time step is odd or even. The criteria for the diffusion terms will be considered in the next section.

THE FORMULATION OF TURBULENT DIFFUSION

For the convection problem choice of an appropriate exchange coefficient is complicated by the wide range of intensities encountered in atmospheric convection, from the development of a modest trade cumulus to violent cumulonimbus associated with severe weather. When a constant exchange coefficient is used, prior knowledge of the expected intensity of convection modeled and the grid spacing influence the choice of an appropriate exchange coefficient. Table 1 is a sampling of the wide range of coefficients used in models similar to the present one. The range covers two orders of magnitude and it is evident that choice of a particular coefficient is somewhat arbitrary. In an attempt to deal with these problems more realistically, a variable exchange coefficient which is a function of the flow field was therefore used.

TABLE 1

Constant exchange coefficients used in numerical convection models. The last two rows apply to the present model.

	$K_{\mathbf{M}}$	$\triangle x$	Δz
Source	$cm^2 sec^{-1}$	m	m
Bykova & Matveev (1966)	50 000	200	200
Takeda (1965)	100 000	2 000	400
Murray (1970)	400 000	200	200
Ogura (1963)	400 000	100	100
Orville (1965)*	400 000	500	200
Chou (1962)	500 000	100	100
Orville & Sloan (1970)*	800 000	100	100
Asai (1964)	1 000 000	500	500
Lilly (1962)	2 500 000	125	125
Murray (1965)	5 000 000	?	?
Takeda (1971)*	5 000 000	1 000	500
Exp. DK	100 000	100	100
Exp. SJK	500 000	100	100

^{*} Difference scheme had significant implicit diffusion.

The coefficient adopted, first suggested by Smagorinsky (1963), is a function of the deformation field and grid separation and varies both in space and time. The form of the coefficient is

$$K_{\mathbf{M}} = (C_0 \Delta)^2 |\text{Def}| \tag{11}$$

where the deformation is defined by

$$\mathrm{Def^2} \; \equiv \; \frac{\partial u \, i}{\partial x_{\, j}} \, \cdot \, \left[\frac{\partial u \, i}{\partial x_{\, j}} \, + \, \frac{\partial u \, j}{\partial x_{\, i}} \right.$$

Here C_0 is a constant which will be discussed shortly, and Δ is the grid point separation of the model. This formulation yields a form

for K_M that is consistent with the 4/3 power law found empirically by Richardson (1926). The dissipation rate, ϵ , is

$$\epsilon = \tau_{ij} \frac{\partial u_i}{\partial x_j}$$

and the stress is parameterized as

$$\tau_{ij} = \kappa_{M} \left[\frac{\partial u_{i}}{\partial x_{i}} + \frac{\partial u_{j}}{\partial x_{i}} \right] ,$$

therefore

$$\epsilon = K_{M} \text{ Def}^{2}$$
 (12)

Eliminating Def between (11) and (12) gives

$$K_{\mathbf{M}} = (C_0 \Delta)^{4/3} \epsilon^{1/3}$$
 (13)

Not only is K_{M} a function of both the grid separation and the deformation field, but from (13) we see that it is also directly related to the dissipation of kinetic energy. For this reason Smagorinsky has suggested that the use of this formulation may in some respects simulate the effects of small scale eddy transfers, and in particular, that the kinetic energy removed by these terms may be similar in amount and distribution to the energy removed by internal friction through the energy cascade process.

Both Lilly (1962) and Smagorinsky (1963) also felt that a formulation such as this would benefit computational stability by suppressing small scale phenomena. In fact, one of the major reasons Lilly sought a variable exchange coefficient was because a constant $K_{\mathbf{M}}$ did not act selectively enough to remove short wave components

which interacted nonlinearly to produce instability. Deardorff (1972) has suggested that $K_H = 3~K_M$. When modeling an unstable boundary layer he found that when K_H was smaller than this there was a tendency for excessive intensity at high wave numbers in the temperature spectrum.

Applying the above information to (1) and (3) and rearranging, we find

$$\frac{d\zeta}{dt}\,-\,g\frac{\partial B}{\partial x}\,-\,K_{\mbox{\scriptsize M}}\nabla^2\,\zeta\,-\,[\frac{\partial^2\,K_{\mbox{\scriptsize M}}}{\partial x^2}\,-\,\frac{\partial^2\,K_{\mbox{\scriptsize M}}}{\partial z^2}]\,[\frac{\partial u}{\partial z}\,+\,\frac{\partial w}{\partial x}]\,-\,2\frac{\partial^2\,K_{\mbox{\scriptsize M}}}{\partial x\partial z}\,.\,..$$

$$\left[\frac{\partial w}{\partial z} - \frac{\partial u}{\partial x}\right] = 0 \tag{1a}$$

$$\frac{d\theta}{dt} + w \frac{\partial \theta_0}{\partial z} - K_H \nabla^2 \theta - \frac{\partial K_H}{\partial x} \frac{\partial \theta}{\partial x} - \frac{\partial K_H}{\partial z} \frac{\partial \theta}{\partial z} = + \frac{\theta_0}{c_p T_0} (\delta_0 Q_1...$$

$$+ \delta_3 Q_2) \qquad (3a)$$

The boundary conditions are the same as those in the previous section, with the additional conditions that

$$K_{\mathbf{M}} = 2(C_0 \Delta)^2 \left| \frac{\partial \mathbf{u}}{\partial \mathbf{x}} \right|$$

on all the boundaries including the symmetry boundary x = 0. As we shall assume the tangential velocities to vanish along the external boundaries, K_M is zero at these boundaries.

This formulation, however, is not without drawbacks. These have to do with the use of Kolmogoroff's similarity hypothesis (Lilly, 1966 and 1967). Kolmogoroff's theory assumes that the grid spacing can properly resolve the largest energy containing scales, in this case the cloud itself. This requirement comes about because it assumes that the grid is within an inertial subrange. The present model has insufficient resolution to meet this criterion. It is questionable whether the eddies involved are isotropic as Kolmogoroff's theory assumes. Additionally, the theory

assumes neutral stratification. Although this condition is not satisfied in the moist experiments, Lilly (1962) attempted to investigate the effect of stratification using a Richardson number approach and found it to be small. Perhaps the most serious deficiency is the lack of the third space dimension in the model.

Smagorinsky (1963) originally suggested that the value of the constant, C_0 , should be the von Kármán constant and he therefore used the value 0.40. Lilly (1962), in his study of convection tested three values, 0.25, 0.50 and 1.00. He found that $C_0 = 0.50$ seemed the best of the three. He based his judgments on computational stability and agreement of certain parameters with similarity theory for convection. Steiner (1973) used a value of $C_0 = 0.42$ in his work. But in a theoretical study Lilly (1967) used Kolmogoroff's similarity theory for turbulence to find that $C_0 = 0.23$ was more appropriate. Later work by Deardorff (1971) gave essentially the same result. The discrepancy between the empirically determined optimum value (0.40 – 0.50) and the theoretical value (about 0.20) can probably be attributed to the inability of the models to properly resolve the inertial subrange. It is obvious, though, that the choice of C_0 is less difficult than the choice of a constant exchange coefficient.

In determining stability criteria including the diffusion term, Ogura and Charney (1962) found

$$\Delta t \leq [(\Delta x)^2 + (\Delta z)^2] / 4 K$$

Using the variable exchange coefficient parameterization which involves nonlinear terms, the above criteria proved insufficient for some experiments. An increase in the numerical factor in the denominator from 4 to 15, however, secured stability. No attempt was made to determine an optimum value for the numerical factor.

RESULTS

Dry Convection

In an attempt to isolate the modifications due to the frictional parameterizations the water phase was completely eliminated thereby reducing the model to that of a dry thermal. The buoyancy then becomes a function of the potential temperature perturbation only, i.e.

$$\mathbf{B} = \theta/\theta_{\mathbf{0}} ,$$

the two source terms, Q_1 and Q_2 , in the temperature and energy equations are zero, and the equations for the various mixing ratios as well as the moisture terms in the energy equation become unnecessary. The relevant system now includes the appropriately modified versions of Eqs. (1), (2), (3), (4) and (8). Additionally, a neutral stratification of the basic state was used to ensure the absence of internal gravity waves. Three experiments were performed. The first (which will be referred to as DD) provides for no diffusion of either momentum and heat. In this case the only energy conversions are from potential to kinetic energy and vice versa. The second experiment uses a constant $K_{\rm M}=1.0\times10^5~{\rm cm}^2~{\rm sec}^{-1}$ (exp. DK) and the third has a variable $K_{\rm M}$ in which $C_0=0.40$ (exp. DV). In both DK and DV, $K_{\rm H}$ was set equal to $K_{\rm M}$. The only difference between the three experiments is the type of frictional parameterization.

Figure 1(a) displays the initial temperature perturbation used in all three experiments. The evolution of temperature and stream function of DD is shown in Figures 1(b) and 1(c) after 10 and 20 minutes of simulation.

Examination of the computer output shows a gradual appearance of small-scale features which are poorly resolved by the finite-difference grid, leading to increasing deterioration of skill in simulation, and eventually to nonlinear instability. This break-up into smaller scales manifests itself most clearly in the vorticity field (Figure 2). While this phenomenon is not very noticeable in the beginning, by 20 minutes it is quite prominent in the core of the updraft and clearly some damping mechanism is needed to prevent this very rapid transfer of energy into smaller scales. The most obvious effect of incorporating friction is to slow the rate of rise of the convective

element as well as to reduce the intensity. The break-up of vorticity into smaller scales is not observed after friction has been incorporated.

It is readily seen from Figures 2(e) and 2(f) that the vorticity maximum ascends somewhat more rapidly in the case of a variable eddy diffusion coefficient and the same applies to the potential temperature maximum (not shown here). The early development of DV resembles DD because the variable K_M is smaller than the constant value used in experiment DK. This is also borne out by Figure 3 which shows the time variation of K_M and how it differs from the constant value used in DK. The average value for K_M shown here is a space average taken over all points in which the value of K_M is within one order of magnitude of its maximum value. Hence, the area over which this averaging takes place varies with time. In Figure 4 these areas are those within the outermost contours. The choice is admittedly arbitrary and is merely an attempt to determine an effective exchange coefficient to compare with the constant value used in DK.

The general form of a diffusion term is

$$\frac{\partial}{\partial x} (K \frac{\partial Q}{\partial x}) + \frac{\partial}{\partial z} (K \frac{\partial Q}{\partial z}) = K \nabla^2 Q + \frac{\partial K}{\partial x} \frac{\partial Q}{\partial x} + \frac{\partial K}{\partial z} \frac{\partial Q}{\partial z}$$

where Q is the quantity being diffused. In DK the last two terms on the right are zero, but for certain grid points in experiment DV the effect of the last two terms was comparable in magnitude to that of the first term and generally hand the same sign as the Laplacian term.

The space distribution of K_M is shown in Figure 4 at 10 and 20 minutes. At most points its value is less than the value 1.0 x 10^5 cm² sec⁻¹ used in DK, but in a small area in and around the core of the bouyant element it exceeds this value and reaches a maximum of 1.7 x 10^5 cm² see⁻¹ after 14 minutes of simulation (Figure 3). Figure 4 also shows that K_M is greatest above and along the sides of the rising temperature bubble, which agrees with the contention by Scorer and Ludlam (1953) that mixing occurs predominantly at the upper and

lateral edges of a cloud, while the core of the cloud is protected from excessive mixing.

Figure 5 gives comparison of potential and kinetic perturbation energies and accumulated kinetic energy dissipation (the potential energy dissipation is not plotted because of the small contribution it made to the energy budget). The potential energy per unit mass as defined here is

$$P_F = -gzB$$

and is therefore a negative quantity which decreases with time as the buoyant element rises; its numerical value is plotted in Figure 5. There is only a modest difference in the development of the potential energy between the three cases. This difference reflects partly a difference in position of the buoyant element and to a lesser extent differences in intensity and shape. The curve corresponding to DV assumes a position intermediate to the other two.

As one would expect the kinetic energy associated with DD is considerably greater than in the case of the two experiments including friction. The difference in kinetic energy between the latter two reflects the increasing efficiency of the variable exchange coefficient in dissipating momentum. Initially this coefficient is relatively small and permits a more vigorous development than in the case of constant K_M ; but as the velocities exceed those of DK, the variable coefficient becomes more effective.

For the first 12 minutes both the kinetic energies and the kinetic energy dissipations of DK and DV are nearly the same. From this time on the difference between the kinetic energy dissipation of DK and DV is smaller than the difference between their kinetic energies. Reference to Figure 4 will help explain the apparent discrepancy. Except over a small area, the variable exchange coefficient is smaller than that used in DK. If the velocity fields were identical, there would be more dissipation over the whole domain for the case of the constant K_M than for the generally smaller variable K_M . Because the latter varies in space, it acts selectively to slow development. It is the

ability of the variable exchange coefficient to locally dissipate momentum effectively where the deformations are large that causes the kinetic energy in DV to be less than that in DK in spite of the fact that the total dissipation is smaller.

An energy residual, the spurious change in total energy due to numerical effects, is displayed in Figure 6. The area above the horizontal axis line indicates creation of excess kinetic energy and the area below indicates that more potential energy was released than was converted to kinetic energy. An additional experiment was run with the variable exchange coefficient parameterization and $K_H/K_M=3$, a value suggested by Deardorff (1972). Because the potential energy is a negative quantity, it was assumed that this stronger reduction in the temperature field would better balance the energy budget. In fact, the energy residual for this experiment was quite similar to DK. Because the ratio of three "overcorrected" the energy budget, $K_H/K_M=2.5$ was chosen for further work. It should be noted that the energy residual is due to numerical effects and that this tuning has little physical basis.

Moist Convection

With the previous set of experiments as a guide, moist convection was modeled using the unmodified set of equations (1)-(8). The bouyancy term now includes the effects of both temperature and suspended liquid (cloud and rain), hence

$$B = \theta/\theta_0 - q_c - q_p.$$

Three experiments were also performed in this category, differing only in the method of parameterizing turbulent diffusion. The first experiment (SJ) includes neither friction nor diffusion of heat and moisture. In the second experiment (SJK) a constant exchange coefficient was used and K_H was set equal to K_M . Because the initial conditions are conducive to vigorous convection, a value for K_M five

times larger than in the previous dry experiment was chosen. In the third experiment (SJV), where the exchange coefficient is variable, the value of C_0 was increased to 0.60 to facilitate comparison with SJK, and K_H was set equal to 2.5 K_M .

The basic state is shown in Figure 7(a); it has a temperature lapse rate which is conditionally unstable and the humidity sounding shows unsaturated air throughout. A cloud will form if the initial perturbation is sufficient to attain a level of free convection (LFC), and saturation must be achieved before the lift provided is dissipated. As discussed by Arnason and Greenfield (1968), the previously used temperature perturbation is insufficient to initiate cloud formation due to the dry-stable stratification and relative humidity well below saturation. In addition to the original temperature perturbation, a relatively humidity perturbation, shown in Figure 7(b) was therefore used to ensure formation of a cloud.

The results of the moist experiments are more difficult to compare and interpret than those for the dry experiments. Because of strong frictional effect during the first few minutes of simulation, attainment of the LFC was delayed somewhat in experiment SJV and quite considerably in SJK. SJ quickly attains its LFC (5 minutes) and develops rapidly due to lack of a braking mechanism. SJK, because of the large initial diffusion of temperature, takes almost 15 minutes to reach the LFC. Initially SJV is similar to SJ because of the very small exchange coefficient, and the LFC is reached after about 7 minutes, but its development soon falls behind that of SJ. Because the rate of development was so different in the three experiments, comparison of results at a fixed simulation time was not considered meaningful, but rather comparison was made when the cloud in each experiment had risen about the same amount and where the stages of development were similar in all three cases.

Figure 8 shows the distribution of temperature and stream function a few minutes after attainment of the LFC. The simulation times for the three experiments are given in the uppermost part of the figure. The edge of the cloud was arbitrarily chosen to coincide with

a cloud mixing ratio of 0.05 g kg⁻¹. Note that the contour intervals differ for each experiment. All three show the development of a secondary circulation reflecting the ocurrence of gravity oscillations. As expected, the temperature perturbation and circulation is strongest in SJ and weakest in SJK due to a prolonged struggle of the convective element to attain the LFC. Regions of negative temperature perturbation appear above and below the cloud. The negative temperature above is due to dry-adiabatic cooling of the rising air whereas below the cloud it is the result of both dry-adiabatic cooling and evaporation of liquid water at the edge of the cloud and in the falling rain below cloud base.

Figure 9 is similar to Figure 8 but shows the convection in a state of vigorous development. After 11 minutes of simulation, the maximum temperature perturbation (more than 7°C) and maximum vertical velocity (14 m sec⁻¹) are both excessive in experiment SJ. The cloud is very narrow as a result of strong advection of drier air into the lower portion of the cloud, but the cloud base remains near 500 m due to rapid fallout and evaporation of rain. Compared to SJ, both SJK and SJV seem to develop a cloud which is more realistic both in shape and size. The effects of both types of friction show up clearly in the form of a broader area of positive buoyancy which in turn leads to a larger circulation cell and a considerably wider cloud.

The evolution of the variable exchange coefficient in the moist convection (Figure 10) is similar to that in the dry convection (Figure 4). The maximum K_M in both dry and moist experiments becomes 60% larger than the constant exchange coefficient before starting to decrease. Also, the average K_M in both cases reaches a maximums that is nearly 50% as large as the constant K_M before decreasing. Both maximum and average variable exchange coefficients are about five times larger in the moist experiment than in the dry experiment. This supports the choice of the constant K_M used in the moist experiment as being five times larger than that used in the dry experiment.

Typically throughout SJV the largest value of $K_{\mbox{\scriptsize M}}$ occurred at both the top and near the bottom of the cloud with a minimum in the

middle near the region of largest temperature perturbation (Figure 11). This agrees with observations made by Warner (1970) who investigated clouds that were more modest than what might be expected from this sounding. He observed strongest turbulence at the cloud tops, and a power spectrum analysis showed greatest dissipation at the top and bottom of the cloud. Physically, an unstable lapse rate develops at the top of the bubble because of the combined effects of heating from the release of latent heat and cooling due to forced dry adiabatic ascent as well as evaporation at the very top of the cloud. This unstable region is the seat of eddy turbulence. Owing to inadequate grid resolution of the model and that $K_{\rm M}$ does not directly take into account the local static stability, the frictional parameterization used in SJV does not accurately model the physical processes, although the variable exchange coefficient seems to be distributed in agreement with the few observations there are.

To show the great difference in growth rates, maxima of potential temperature perturbation, vertical velocity, liquid water content and cloud width are presented as functions of time in Figure 12. Note the almost explosive development of core values when no friction is present. In takes about 15 minutes of struggling for the cloud in SJK to get organized and for the temperature to start to increase. The maximum temperature perturbation in SJV reaches about 2.5°C after about 15 minutes of simulation and then remains nearly constant. Because the release of latent heat controls the dynamics of the convection, there is a lag between the time the latent heat is released (as shown by the temperature maxima) and the time it is reflected in the velocity field. This lag is evident for both SJK and SJV; in the latter, the maximum velocity levels off about three minutes after the temperature. The evolution of the maximum liquid water content (LWC) in all three experiments is similar to that of the maximum temperature perturbation and vertical velocity but it lags both. The lateral expansion of the cloud in both SJ and SJK is quite similar. But it should be noted that during the first 11 minutes the cloud in SJK was fighting to get organized while that in SJ was developing explosively. The cloud in SJV is wider than either SJ or SJK and at

the time the experiments were terminated the width of the cloud in SJV was nearly 200 m larger than that in SJK.

An investigation of both the energetics and dynamics of convective motion is necessary to better evaluate the frictional parameterizations. In the dry convection there was a balance between the released potential energy and its conversion to kinetic energy. In moist convection all the energy terms are much larger, and the main balance is between the potential energy and latent heat release. In comparison the kinetic energy is small, but it is important in the sense that it reflects the intensity of the flow which provides the mechanism for uplift that enables potential energy to increase and latent heat to be released.

The variation of the energy terms for the moist experiments is presented in Figure 13. Clearly, all of the terms in SJ increase at an unrealistic rate. The rate of increase of potential energy and latent heat release is similar for both SJK and SJV once the former has started to grow. The important difference is in the kinetic energy term for SJV where after 15 minutes the increase in kinetic energy slows considerably. It is apparent that the variable exchange coefficient is modifying the growth of the cloud by a feedback mechanism that is not possible when the friction is parameterized using a constant K_M . The dissipation terms are not shown because they were quite small compared to the other terms in the energy budget. The evolution of the kinetic energy dissipation was similar to the dry experiments: a smaller amount of total dissipation in SJV was sufficient to keep the kinetic energy smaller than in SJK.

Although numerically small, the importance of the frictional terms can be seen by an examination of the buoyancy terms after the onset of vigorous convection (Figure 14). For each experiment the resultant buoyancy is partitioned into contributions due to the temperature perturbation, suspended liquid, and dynamic pressure. The two experiments with friction are vastly different from SJ but similar to each other. In SJ the extremely large resultant bouyancy is dominated by the pressure term. The resultant bouyancy is more than an order of magnitude smaller in both SJK and SJV. Although the

thermal term tends to dominate in the experiments with friction, the resultant buoyancy is relatively small due to compensation among the various components.

The true test of a model is its ability to simulate nature. Aircraft observations of clouds associated with the sounding used in these experiments showed maximum temperature perturbations of 1.5°C and liquid water content of 3 g kg⁻¹. Actual values may well have been larger than these as the airplane traverses may not have encountered the true maxima. The rate of cloud toporise was found to be 6-7 m sec⁻¹. Murray (1971) indicates that a good rule of thumb is that the maximum updraft velocity is about twice the rise rate of the cloud top. This would indicate that the maximum updrafts were around 10-15 m sec⁻¹.

Comparing these observations with Figure 12, it would seem that SJV best simulated the cloud development. Its maximum temperature perturbation reached 2.5°C which was reasonably close to the observed temperature excess. SJK (4°C) was too large and still increasing and SJ was completely unrealistic. The maximum updraft in SJV (5 m sec⁻¹) remained too small throughout the experiment. But if C₀ had not been increased from 0.40 to 0.60 to enable comparison with the constant K_M, SJV would probably have produced a large updraft. SJK had a maximum vertical velocity of 7 m sec⁻¹ and was still increasing when the experiment was terminated and it is possible that the updraft would have increased beyond the observed values. SJV had a maximum LWC of 3.5 g kg⁻¹ which was closer to observations than either SJ or SJK. Based on Figure 12, it seems that the cloud in SJV had reached a steady state. Both the temperature excess and the updraft had leveled off for the last few minutes of the experiment. It is possible that this was also the case for the LWC. At this same time the cloud continued to rise and spread out. Had it not been for the rigid upper boundary at 3 000 m. experiment SJV might well have produced a cloud similar in size to those observed.

SUMMARY AND CONCLUSIONS

The case studies reported here show that numerical simulation of moist convection in an environment conducive to convection in nature will show excessive cloud development if turbulent eddy diffusion is not taken into account. They also show that parameterized eddy diffusion, making use of either a constant or variable exchange coefficient, is capable of preventing such a development, and that the model then simulates a cloud which has a natural look compared with the unrealistically narrow cloud of a non-viscous model.

Judging from the overall features of the simulated clouds, the two types of parameterizations appear to give similar results. However, the variable exchange coefficient has the ability to selectively remove energy where deformations in the velocity field are largest and as a result produce maximum entrainment near the top and edges of the cloud in accordance with observations. Another difference between the two is apparent in the initial rate of cloud development. The use of a constant eddy coefficient, because of its immediate suppression of buoyancy, greatly delays the initial cloud development. This, however, is not the case for a variable exchange coefficient. Since it is proportional to velocity gradients, it has little effect on the early cloud development which is therefore similar to the non-viscous case. Moreover, maximum values of temperature excess, liquid water content, and cloud width were better predicted with a variable coefficient.

It is therefore tentatively concluded from these case studies that a variable exchange coefficient leads to a more realistic cloud simulation and is therefore to be preferred over a constant coefficient.

APPENDIX A

List of Symbols

- a threshold value for $\rho_0 q_c$, above which a part of the cloud is converted to rain through autoconversion (set equal to 0.5 x 10^{-7} g cm⁻³)
- B buoyancy term
- C₀ constant in variable eddy exchange formulation
- C_1 constant in expression for fall velocity (set equal to 2.17 x 10^{-4})
- C₂ constant in expression for autoconversion (set equal to 10⁻³)
- C_3 constant in expression for coalescence (set equal to 6.98 x 10^{-10})
- C₄ constant in expression for evaporation of raindrops (set equal to 1.35×10^{-10})
- c_p specific heat per unit mass at constant pressure

$$\frac{d}{dt}$$
 $\frac{\partial}{\partial t}$ + $u\frac{\partial}{\partial x}$ + $w\frac{\partial}{\partial z}$

Def deformation tensor

dσ a volume element

E collection efficiency (set equal to 1.0)

g gravitational acceleration

H source function for saturation mixing ratio and part of source term due to condensation, also vertical extent of the model

K exchange coefficient

K_E kinetic energy per unit mass

K_H eddy exchange coefficient for heat

K_M eddy exchange coefficient for momentum

L latent heat of evaporation, also half the horizontal extent of the model

N parameter for size distribution of raindrops (intercept of Marshall-Palmer curve) (set equal to 10⁷)

p	dynamic pressure
${\bf P_E}$	potential energy per unit mass
Q_1	source term due to condensation or evaporation of cloud
~ 1	drops
Q_2	source term due to evaporation of raindrops
q	total specific water content
q_{c}	specific water content of cloud
q_p	specific water content of precipitation
q_{s}^{p}	saturation mixing ratio
q_v	mixing ratio of water vapor
R	gas constant for moist air
R_{v}	gas constant for water vapor
S_0^{ν}	source term due to condensation or evaporation of cloud
•	drops
S_1	source term due to autoconversion
S_2	source term due to coalescence
S_3	source term due to evaporation of raindrops
S_4	source term due to fallout of rain
T	absolute temperature
t	time
u	horizontal component of velocity
V	precipitation fall velocity
w	vertical component of velocity
X	horizontal coordinate
Z	vertical coordinate
γ	environment lapse rate
T_d	dry adiabatic lapse rate
$T_{\mathbf{m}}$	moist adiabatic lapse rate
$\delta_{\mathbf{i}}$	a tag $(i = 0, 1, 2, 3)$
$\epsilon^{^{1}}$	kinetic energy dissipation rate
ζ	vorticity for flow in the xz plane
θ	potential temperature
μ	coefficient of dynamic viscosity
$\mu_{ m e}$	coefficient of eddy viscosity

v kinematic coefficient of viscosity

 ρ density of air

φ geopotential

 τ_{ii} stress tensor component

ψ stream function

$$\nabla^2 \qquad \frac{\partial^2}{\partial x^2} + \frac{\partial^2}{\partial z^2}$$

 $\Delta x, \Delta z$ horizontal and vertical grid separation

 $\Delta \qquad \Delta x.\Delta z)^{1}/_{2}$

APPENDIX B

Definition of source terms

The microphysical parameterization is that due to Kessler (1969). In this parameterization the liquid water content is divided into two categories; one consists of small suspended cloud droplets that move with the air, the other of large drops which move horizontally with the air but fall relative to the air (precipitate) as a result of gravity. This precipitating water is assumed to have the Marshall-Palmer distribution. Kessler's theory gives the following relation for the fall velocity V in terms of the specific water content of precipitation:

$$V = C_1 \left[\frac{\rho_0 q_p}{N} \right]^{0.125}$$

The source term S_0 for condensation or evaporation of cloud drops is definided by

$$S_0 = -Hw$$

where

$$H = \frac{g}{R} \left[\frac{0.622L - c_p T_0}{c_p T_0^2 + \delta_0 L^2 q_{s_0}^2 / R_v} \right] q_{s_0}$$

Once the cloud mixing ratio exceeds a critical value, a/ρ_0 , the source term S_1 converts cloud water to rain (autoconversion); it is given by

$$S_1 = C_2 [q_c - a/\rho_0]$$

The source term for coalescence is

$$S_2 = C_3 E N^{0.125} q_c (\rho_0 q_p)^{0.875}$$

where E is the collection efficiency and N is a parameter for the size distribution of raindrops based on the Marshall-Palmer distribution, and that for evaporation of precipitation is

$$S_3 = C_4 N^{0.35} (q_S - q_V) (\rho_0 q_p)^0$$
:65

where q_s is found from:

$$\frac{\mathrm{dq}_{\mathrm{S}}}{\mathrm{dt}} = -\mathrm{Hw}$$

In the case of cloud droplets, evaporation produces an instantaneous adjustment to maintain the relative humidity at 100%. For raindrops the evaporation is not instantaneous and rain can be present in areas that are not saturated.

The fallout of rain is given by:

$$S_4 = \frac{\partial}{\partial z} [q_p V]$$

Latent heat is both released by condensation and removed by evaporation. This must be accounted for as a source term in the temperature equation:

$$Q_1 = -L S_0$$

Latent heat loss by evaporation of rains is given by:

$$Q_2 = -L S_3$$

The decision on which terms are retained is based on the following criteria:

$$\begin{split} &\delta_0 = 1 \text{ if } q_c > 0 \text{ or } q_v = q_s \text{ and } w > 0 \\ &\delta_0 = 0 \text{ if } q_v < q_s \text{ or } q_v = q_s \text{ and } w \leqslant 0 \\ &\delta_1 = 1 \text{ if } q_c > a/\rho_0 \\ &\delta_1 = 0 \text{ if } q_c < a/\rho_0 \\ &\delta_2 = 1 \text{ if } q_p > 0 \text{ and } q_c > 0 \\ &\delta_2 = 0 \text{ if } q_p < 0 \text{ or } q_c = 0 \\ &\delta_3 = 1 \text{ if } q_p > 0 \text{ and } q_v < q_s \\ &\delta_3 = 0 \text{ if } q_p > 0 \text{ and } q_c > 0 \end{split}$$

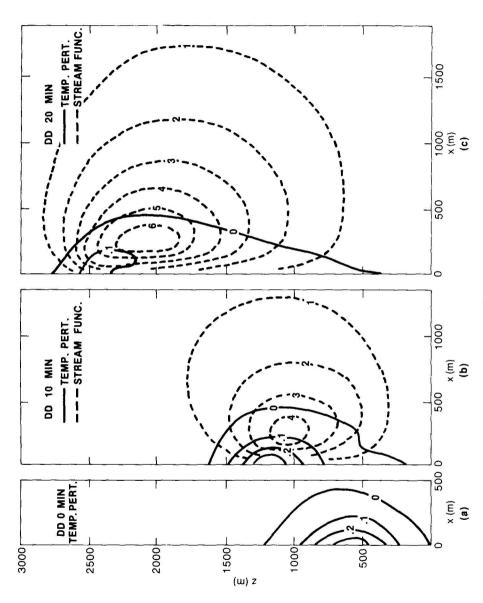


Figure 1. Temperature perturbation ($^{\circ}$ C) and stream function (cm² sec⁻¹ x 10⁻⁶). (a) Initial temperature perturbation used for all experiments, (b) DD after 10 minutes of simulation and (c) DD after 20 minutes of simulation.

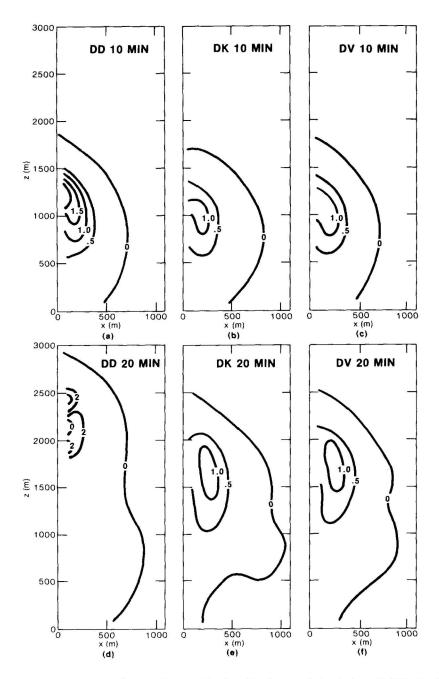


Figure 2. Vorticity ($\sec^{-1} \times 10^{-2}$). (a) DD after 10 minutes of simulation, (b) DK after 10 minutes of simulation, (c) DV after 10 minutes of simulation, (d) DD after 20 minutes of simulation (e) DK after 20 minutes of simulation and (f) DV after 20 minutes of simulation.

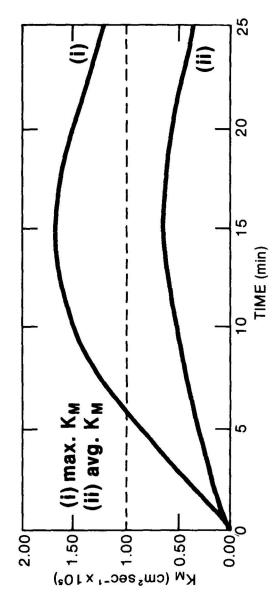


Figure 3. Time evolution of the variable exchange coefficient (cm² sec⁻¹ x 10⁵) in DV.

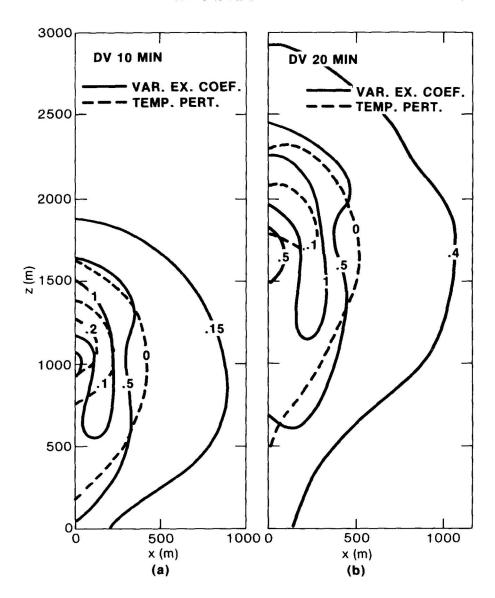


Figure 4. Variable exchange coefficient (cm² $sec^{-1} \times 10^5$) and temperature perturbation (°C) in DV: (a) after 10 minutes of simulation and (b) after 20 minutes of simulation.

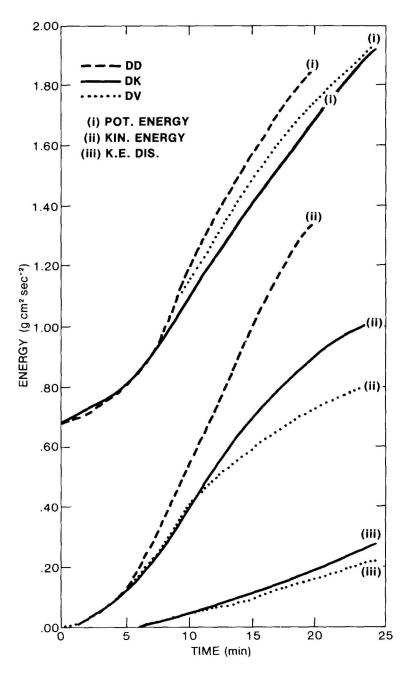


Figure 5. Time evolution of energy terms (g cm 2 sec $^{-2}$) for experiments simulating dry convection: (i) absolute of the potential energy, (ii) kinetic energy and (iii) accumulated kinetic dissipation.

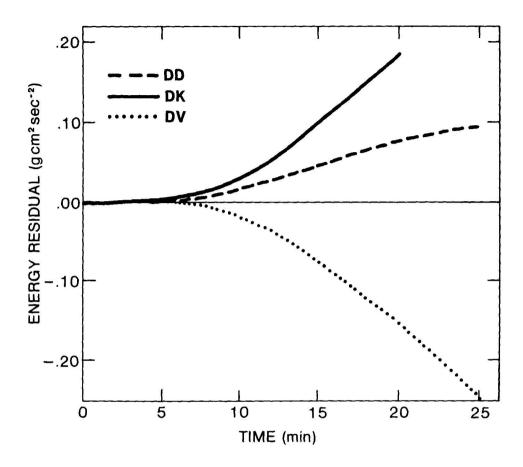


Figure 6. Time evolution of the energy residual (g cm² sec⁻²).

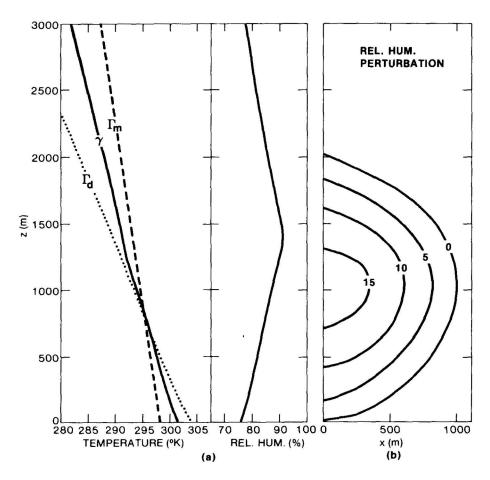


Figure 7. Initial conditions for the experiments simulating moist convection. (a) Basic state temperature (γ) with a dry adiabat (T_d) and a moist adiabat (T_m) for reference, and the basic state relative humidity profile and (b) initial relative humidity perturbation used in all the moist experiments.

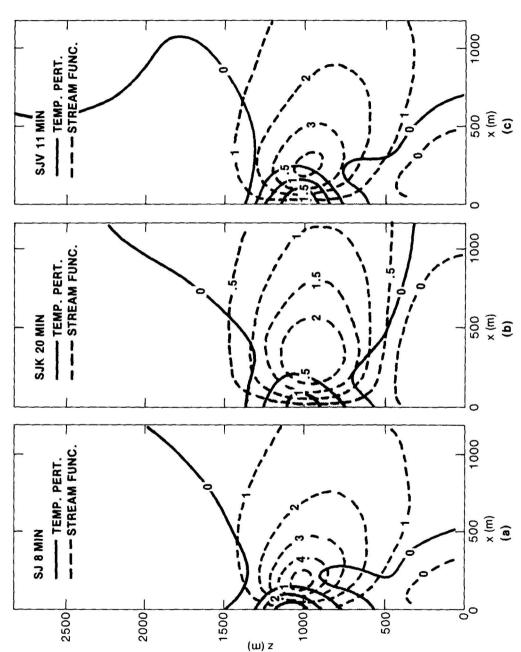


Figure 8. Temperature perturbation ($^{\circ}$ C), stream function ($^{\circ}$ Ca) sec $^{-1}$ x 10 $^{-6}$) and cloud outline (shaded). (a) SJ after 8 minutes of simulation, (b) SJK after 20 minutes of simulation and (c) SJV after 11 minutes of simulation.

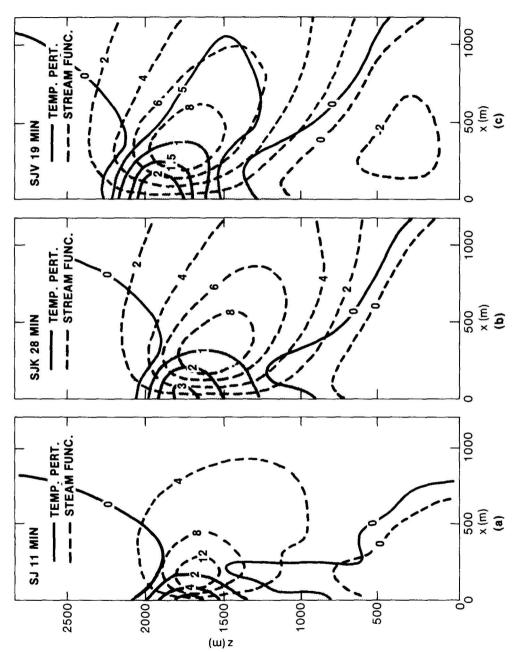


Figure 9. Same as Figure 8. (a) SJ after 11 minutes of simulation, (b) SJK after 28 minutes of simulation and (c) SJV after 19 minutes of simulation.

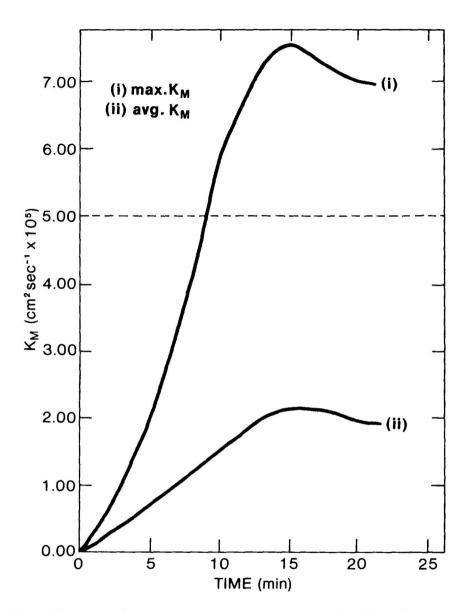


Figure 10. Time evolution of the variable exchange coefficient (cm² sec⁻¹ x 10⁵) in SJV.

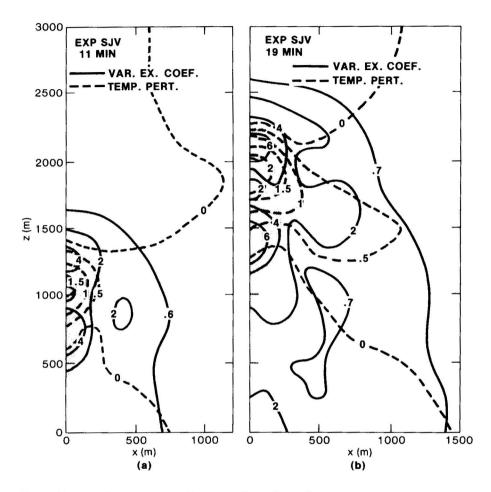


Figure 11. Variable exchange coefficient (cm 2 sec $^{-1}$ x 10 5), temperature perturbations (°C) and cloud outline (shaded) in SJV: (a) after 11 minutes of simulation and (b) after 19 minutes of simulation.

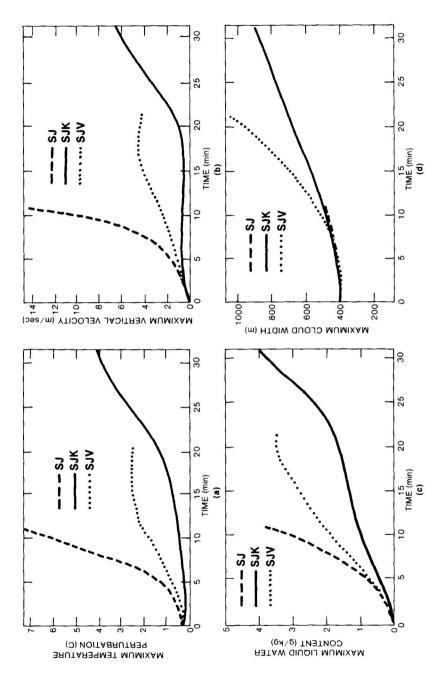


Figure 12. Time evolution of the maximum (a) temperature perturbation (°C), (b) vertical velocity (m sec-1), (c) liquid water con tent (g Kg⁻¹) and (d) cloud width (m).

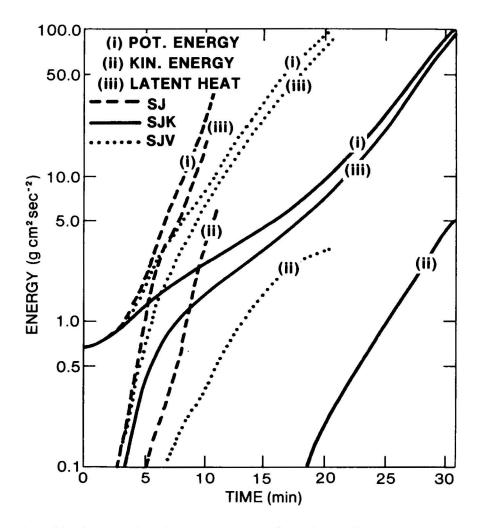


Figure 13. Time evolution of energy terms (g cm 2 sec $^{-2}$ x 10^{-3}) for the experiments simulating moist convection: (i) absolute value of the potential energy, (ii) kinetic energy and (iii) latent heat.

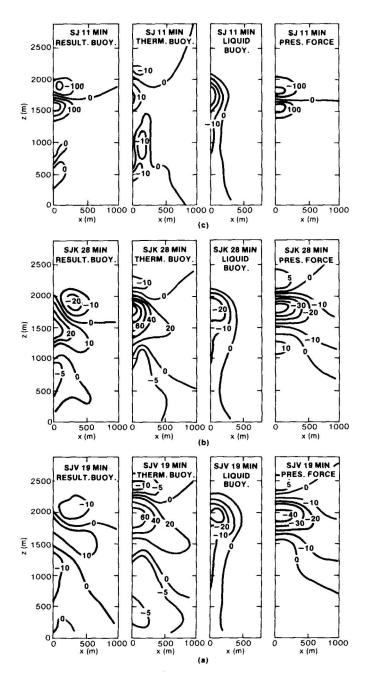


Figure 14. From left to right: the resultant buoyancy, the thermal bouyancy, the liquid buoyancy and the effect of the pressure perturbation. The units are arbitrary, but a value of 10 corresponds to a temperature perturbation of about 0.30°C. (a) SJ after 11 minutes of simulation, (b) SJK after 28 minutes of simulation and (c) SJV after 19 minutes of simulation.

ACKNOWLEDGMENTS

This research was carried out while Francis P. Richards held a UCAR graduate fellowship in atmospheric science, and some of the computer time was provided by the National Center for Atmospheric Research which is sponsored by the National science Foundation. It was also supported in part by the Atmospheric Science Section of the National Science Foundation under Grant A032330-X02. Thanks are extended to miss Sally Young for typing the manuscript.

BIBLIOGRAPHY

- ÁRNASON, G., 1974. On the problem of multivalued pressure in the theory of convection. *Journal of the Atmospheric Sciences*, 31: 1169-1171
- ÁRNASON, G. and R. S. GREENFIELD, 1968. Relationships between tropical precipitation and kinematic cloud models. Final Report, Contract DA 28-043 AMC 01212(E), The Travelers Research Center, Inc., Hartford, Connecticut.
- ÁRNASON, G., R. S. GREENFIELD and E. A. NEWBURG, 1968. A numerical experiment in dry and moist convection including the rain stage. *Journal of the Atmospheric Sciences*, 25: 404-415.
- ARNASON, G. and E. A. NEWBURG, 1966. Relationships between tropical precipitation and kinematic cloud models. *Report No. 8*, Contract DA 28-043 AMC 01219(E), The Travelers Research Center, Inc., Hartford, Connecticut.
- ASAI, T., 1964. Cumulus convection in the atmosphere with vertical wind shear: A numerical experiment. *Journal of the Meteorological Society of Japan*, 42: 245-259.
- BYKOVA, L. R. and L. T. MATVEEV, 1966. Evolution of cloud and temperature fields in a moving cyclone (A numerical experiment). Akademiia Nauk SSSR. Izvestija. Atmospheric and Oceanic Physics, 2: 905-919.
- CHOU, H.P., 1962. Development of cumulus clouds. Akademiia Nauk SSSR. Bulletin of the Academy of Sciences of the U.S.S.R. Geophysics Series, 4: 358-363.
- DEARDORFF, J. W., 1971. On the magnitude of the subgrid scale eddy coefficient. *Journal of Computational Physics*, 7: 120-133.
- DEARDORFF, J. W., 1972. Numerical investigation of neutral and unstable planetary boundary layers. *Journal of the Atmospheric Sciences*, 29: 91-115.
- DRAKE, R. L., P. D. COYLE and D. P. ANDERSON, 1974. The effect of nonlinear eddy coefficients on rising line thermals. *Journal of the Atmospheric Sciences*, 31: 2046-2057.
- KESSLER, E., 1969. On the distribution and continuity of water substance in atmospheric circulations. American Meteorological Society, *Meteorological*

- Monographs, No. 10, Boston, Massachusetts.
- LILLY, D. K., 1962. On the numerical simulation of buoyant convection. *Tellus*, 14: 148-172.
- LILLY, D. K., 1966. On the application of the eddy viscosity concept in the inertial sub-range of turbulence. National Center for Atmospheric Research *Manuscript No. 123*, Boulder, Colorado.
- LILLY, D. K., 1967. The representation of small-scale turbulence in numerical simulation experiments. *Proc. IBM Sci. Comp. Symp. on Environ. Sci.*, Nov. 14-16, Yorktown Heights, New York.
- MURRAY, F. W., 1965. Some problems associated with the modeling of moist atmospheric thermal convection. *Proc. Internat. Conf. on Cloud Physics*, Tokyo and Sapporo, Japan, IAMAP/WMO, Sci. Council of Japan and Met. Soc. of Japan, pp. 6-10.
- MURRAY, F.W., 1970. Numerical models of a tropical cumulus cloud with bilateral and axial symmetry. Monthly Weather Review, 98: 14-28.
- MURRAY, F. W., 1971. Humidity augmentation as the initial impulse in a numerical cloud model. *Monthly Weather Review.* 99: 37-48.
- OGURA, Y. 1963. The evolution of a moist convective element in a shallow, conditionally unstable atmosphere: A numerical calculation. *Journal of the Atmospheric Sciences*, 20: 407-424.
- OGURA, Y. and J.G. CHARNEY, 1962. A numerical model of thermal convection in the atmosphere. *Proc. Internat. Symp. Num. Wea. Pred.*, Tokyo, Met. Soc. of Japan, pp. 431-452.
- ORVILLE, H. D. 1965. A numerical study of the initiation of cumulus clouds over mountainous terrain. *Journal of the Atmospheric Sciences*, 22: 684-699.
- ORVILLE, H. D. and L. J. SLOAN, 1970. Effects of higher order advection techniques on a numerical cloud model. Monthly Weather Review, 98: 7-13.
- RICHARDSON, L. F., 1926. Atmospheric diffusion shown on a distance-neighbour graph. *Proc. Roy. Soc.*, 110: 709-737.
- SCORER, R.S. and F.H. LUDLAM, 1953. Bubble theory of penetrative convection. Quarterly Journal of the Royal Meteorological Society, 79: 94-103.
- SHUMAN, F.G., 1957. Numerical methods in weather prediction: II. Smoothing and filtering. Monthly Weather Review, 85: 357-361.
- SMAGORINSKY, J., 1963. General circulation experiments with the primitive equations: I. The basic experiment. *Monthly Weather Review*, 91: 99-164.
- STEINER, J. T., 1973. A three-dimensional model of cumulus cloud development. *Journal of the Atmospheric Sciences*, 30: 414-435.
- TAKEDA, T., 1965. The downdraft in a convective shower cloud: a numerical calculation. *Proc. Internat. Conf. on Cloud Physics*, Tokyo and Sapporo, Japan, IAMAP/WMO, Sci. Council of Japan and Met. Soc. of Japan, pp. 30-33.
- TAKEDA, T., 1971. Numerical simulation of a precipitating convective cloud: The formation of a 'long-lasting' cloud. *Journal of the Atmospheric Sciences*, 28: 350-376.

- WARNER, J., 1970. The microstructure of cumulus clouds: III. The nature of the updraft. *Journal of the Atmospheric Sciences*, 27: 682-688.
- WILHELMSON, R., 1974. The life cycle of a thunderstorm in three dimensions. Journal of the Atmospheric Sciences, 31: 1629-1651.
- WILHELMSON, R. and Y. OGURA, 1972. The pressure perturbation and the numerical modeling of a cloud. *Journal of the Atmospheric Sciences*, 29: 1295-1307.